Age-based approach to characterize the dynamics of cellular processes

Elad Noor*†[a], Kirill Jefimov[b], Ersilia Bifulco[b], and Evgeny Onischenko*†[b]

[a]Department of Plant and Environmental Sciences, Weizmann Institute of Science, Israel
[b]Department of Biological Sciences, University of Bergen, Norway

September 14, 2025

1 Abstract

Cells continuously produce and degrade multiple small and large molecules, essential for maintaining homeostasis. The study of this dynamics has gained momentum since the development of pulse-chase methods, in which cellular components are labeled with isotopic or fluorescent tracers to assess properties such as turnover rates or half-lives. Standard analyses, however, often rely on simplifications such as that molecules represent a homogeneous and immediately labeled population, which does not always hold true. Here, we present a rigorous analytical framework that refocuses the interpretation of dynamic labeling experiments toward the distribution of metabolic ages, defined as the time molecules have spent within a cell. We demonstrate how this approach ubiquitously captures different aspects of dynamic behavior, including delayed labeling and complex degradation patterns, and is less prone to biased interpretations. We further introduce a general compartmental modeling approach to quantify metabolic age distributions and to test hypotheses about the organization of metabolic networks and show that metabolic ages can be quantified by dynamic labeling requiring minimal assumptions. The utility of this framework is demonstrated by quantifying metabolic ages and determining the kinetic pool structure of budding yeast proteins at optimal and suboptimal growth temperatures, revealing, for example, distinct kinetic populations of ribosomal proteins. In addition, based on the previously published data on nuclear pore complex assembly, we exemplify how age interpretation of dynamic labeling can enable characterizing the order and time scale of the cellular processes.

2 Significance Statement

To be functional, cells must balance the production and degradation of biological molecules. This is often studied using tracers, compounds that label newly-made molecules. However, determining parameters of these processes, such as degradation rates, is not easy and is challenged by non-instantaneous labeling and complex degradation patterns. Here, we describe a generic framework for interpreting results of dynamic labeling experiments based on the concept of metabolic age, the time that the tracer has spent in the metabolic system. Using a custom Python package for metabolic models, we illustrate how this framework enables us to standardize the determination of various dynamic parameters of metabolism and to use age to analyze order and duration of cellular processes.

3 Introduction

Living cells are incredibly complex dynamic systems with thousands of different types of molecules that are constantly produced and degraded [37]. The stability of RNAs and proteins, in particular, determines their abundance and quality and is important for maintaining cellular hemostasis [4, 44]. Cells may employ complex regulatory mechanisms to control this dynamics. For example, the stability of proteins and RNA can be influenced by chemical modifications or subcellular localization [36, 43, 46].

However, it is no simple task to characterize these dynamic effects. One common approach is based on dynamic labeling under steady state conditions (that is, constant cellular growth conditions) when the content of *metabolic tracers* – labeled versions of nutrients – incorporated into the target molecules is measured over time after the tracer was added externally [4, 12–14, 38, 40]. A canonical example are isotopically labeled amino acids that are used to determine the lifespan and turnover of cellular proteins by measuring the dynamics of their incorporation into the proteins analyzed [22]. Similarly, ^{13}C-glucose is used to investigate phosphosugar exchange in central carbon metabolism [21, 30]. Dynamic labeling can also be implemented with a variety of florescence-based approaches [42, 46, 48].

Common to all these strategies is the way parameters such as *lifespan* – which measures the duration of existence, *turnover* – measuring the exchange rate, or *half-life* – the time it takes to replace half of the molecular pool, are determined, i.e., typically by assuming instantaneous labeling of the analyzed molecules and that they can be represented by a single well-mixed pool with a constant degradation rate [35]. However, these conditions are not always met. For example, non-exponential degradation patterns have previously been reported for RNA and proteins [4, 26], while a significant delay in protein labeling by amino acids and other metabolic tracers has been described in unicellular and multicellular organisms [17, 20, 24, 33]. In addition, in many cases the analyzed system does not retain constant size, as, for example, growing cell cultures. How these factors influence dynamic labeling and how they can be

*E.N. and E.O. contributed equally to this work
†To whom correspondence should be addressed. E-mail: evgeny.onishchenko@uib.no or elad.noor@weizmann.ac.il

accounted for has yet to be rigorously addressed.

In other fields that also study complex dynamic systems, such as geophysics, hydrology, and biogeochemistry, the concept of *age distribution* was introduced to describe a variety of dynamic characteristics related to the exchange of water in natural reservoirs [3, 15, 16]. Age is defined as the time that has passed since the particles in question (e.g. molecules of water or carbon dioxide) entered the dynamic system. The probability distribution of the ages allows us to describe the dynamic properties of such systems in the most general terms and with minimal assumptions [3].

Here, we adapt the concept of age distribution to probing the dynamics of biological systems using dynamic labeling approaches. We show that the results of steady-state dynamic labeling experiments ubiquitously reflect the age distribution of the tracer in the observed molecular pool, the *metabolic age distribution*. We also demonstrate how this interpretation allows one to account for a variety of confounding factors in dynamic labeling experiments and highlight their main limitations.

As a starting point, in Sections 4.1-4.2 we define the metabolic age distribution and demonstrate its equivalence to the observed steady-state labeling dynamics. In Sections 4.3-4.5 we use this equivalence and a generic "black-box" representation of metabolic systems to connect the observed labeling dynamics with parameters including the residence time, decay rate, or age of observed molecules under conditions of delayed labeling, complex degradation patterns, and cell proliferation. To facilitate the quantification of dynamic properties in real experiments, in Sections 4.6-4.7, we introduce an alternative representation of steady-state metabolic systems through compartmental models (CM) that subdivide a metabolic system into distinct parts that represent physical compartments or biochemical reaction pools. Finally, in Sections 4.8-4.9, we illustrate the practical application of age-based interpretation and CMs by quantifying the dynamic parameters of the yeast proteome at optimal and suboptimal growth temperatures and by analyzing the order and timescale of the yeast nuclear pore complex assembly.

4 Results

4.1 Conventions about steady-state labeling dynamics and the definition of dynamic parameters

To mathematically describe dynamic labeling experiments, we will use strict definitions and assumptions about the properties of the biological systems analyzed. Here, we refer to biological systems (for example, cell cultures or animal tissues) also as *metabolic systems* or *dynamic systems*. Specific sets of metabolites within the metabolic system are called *metabolic pools*, for example, vacuolar and protein-borne amino acid pools. The pools that are experimentally analyzed are called *observed* and they are *unobserved* otherwise, and together comprise a *whole* metabolic system. We consider that the metabolic systems are in a dynamic steady state during the experiments, i.e. that all of their biochemical parameters, including the relative sizes of metabolic pools or the rates of biochemical reactions, remain constant. These conditions can be met, for example, in nondividing or exponentially growing cell cultures that remain in the same culturing conditions throughout the entire period of the labeling experiment or when cells are examined over sufficiently short time intervals where their metabolism remains essentially unchanged.

Throughout the work, we focus on a specific dynamic labeling scenario in which an essential (i.e., one that must be supplied externally) unlabeled *metabolic tracer* is instantly replaced at time $t = 0$ with its labeled variant during the *labeling pulse* period in the external environment without disrupting steady-state cell metabolism (Figure 1B). The readout of such experiments is the *labeling dynamics(curve)* $f(t)$, defined as the fraction of the unlabeled tracer that remains in cellular metabolic pools at times $t > 0$ after the labeling pulse (Figure 1B). The metabolic tracer can represent an entire molecule, a chemical group, or a single atom, as long as it can be experimentally detected and quantitatively compared to the unlabeled variant. Crucially, the two variants must be metabolically indistinguishable (or the effect of swapping them is negligible). A common example is when stable isotope-coded nutrients play the role of tracers and their relative abundance is determined by quantitative mass spectrometry. Notably, this standard scenario can be tailored to other types of dynamic labeling, including isotopic labeling with non-essential nutrients, pulse-chase labeling with radioisotopes, or using genetically encoded fluorophores as tracers, which we address in Section S1.2.

We also strictly define the dynamic properties of metabolic systems. The term *metabolic age* ($\mathcal{A}$) defines the time that has passed since the tracer particles entered the metabolic system, while *residence time* ($\mathcal{T}$) is defined as the time spent within the whole system or its pools between the moment of entry and the moment of exit (Figure 1A). Note that the term *transit time* is sometimes used in the literature to convey the same meaning [3, 15, 16]. The term *decay rate* (κ) defines the fractional escape rate of specific subsets of tracer particles from the metabolic system. Finally, we define *half-life* ($t_{1/2}$) as the time during which half of the traced particles were replaced with the tracer $f(t_{1/2}) = 1/2$.

We consider metabolic ages and residence times to be random variables described by probability density functions (PDF), $p_{\mathcal{A}}(t)$ and $p_{\mathcal{T}}(t)$. In steady state, these PDFs define constant probability distributions, for example, as shown in Figure 1A. We can also define them through the cumulative distribution functions (CDF), that is, the fraction of particles younger than t among all particles within the system – $P_{\mathcal{A}}(t)$ and the fraction of particles spending in the system less than time t among all particles leaving the system – $P_{\mathcal{T}}(t)$. As is true for any probability distribution, CDF and PDF are related through differentiation, e.g.:

$$p_{\mathcal{A}}(t) = \dot{P}_{\mathcal{A}}(t) \tag{1}$$

where the dot above a function symbol represents its time derivative, i.e. $\dot{g} = dg/dt$. Note that we use the

variable t to represent both age and time, although they are not exactly the same. However, this duality has a reason that will become clear in the following section.

4.2 Steady-state labeling dynamics defines metabolic age distribution

We can now demonstrate that, in steady-state dynamic labeling experiments, the labeling dynamics and the metabolic age distribution are unequivocally connected. Consider the time $t = 0$ at which the labeled metabolic tracer is introduced. Since it was unavailable before time $t = 0$, all its instances are always younger than the duration of the metabolic pulse, while the unlabeled instances are necessarily older (Figure 1B). In other words, the fraction of labeled/unlabeled tracer and the fraction of its young/old instances are, in fact, two sides of the same coin. As this relationship is valid for any time $t > 0$, we can conclude that the labeled fraction of the metabolic tracer in the measured molecular pool(s) defines the cumulative distribution (CDF) of its *metabolic age* $P_{\mathcal{A}}(t)$, that is, the probability that the time it spent in the metabolic system is shorter or equal to t (Figure 1B). Since these two fractions add up to 1, we can now write:

$$P_{\mathcal{A}}(t) = 1 - f(t) \tag{2}$$

The metabolic age distribution itself can be found using the relation to CDF in Equation 1 showing that it is simply defined by the slope of the labeling curve:

$$p_{\mathcal{A}}(t) = -\dot{f}(t)\,. \tag{3}$$

As a consequence, since $p_{\mathcal{A}}(t)$ takes only nonnegative values, steady-state labeling dynamics $f(t)$ must be a nonincreasing function. Therefore, if the unlabeled fraction increases at some point, the system must be out of steady state (Figure 2).

Furthermore, using the age-based interpretation and Equation 2, we can see that the half-life $t_{1/2}$ (the time point at which the tracer labeling function reaches 50%) defines the median metabolic age, that is, $P_{\mathcal{A}}(t_{1/2}) = \frac{1}{2}$. This provides a new interpretation for this metric commonly used in dynamic labeling experiments [17, 35] (Figure 3). Notably, the mean metabolic age turns out to be relatively simple to calculate as well and is equal to the area under the labeling curve (see Appendix S1.3.1):

$$\bar{\mathcal{A}} = \int_0^{\infty} f(t)dt\,. \tag{4}$$

Since the median and mean values of metabolic age depend only on the shape of the labeling curve, they can be determined directly from the labeling data (Figure 3). For example, the mean age ($\bar{\mathcal{A}}$) can be estimated geometrically by dividing the area under the curve into trapezoids and calculating their total area (Appendix S1.8.2). The mean age can also be characterized conditionally, focusing on a specific range of metabolic ages (Appendix S1.3.7).

In conclusion, the metabolic age distribution of the traced metabolite is unequivocally related to steady-state labeling dynamics, which makes it quantifiable without prior assumptions.

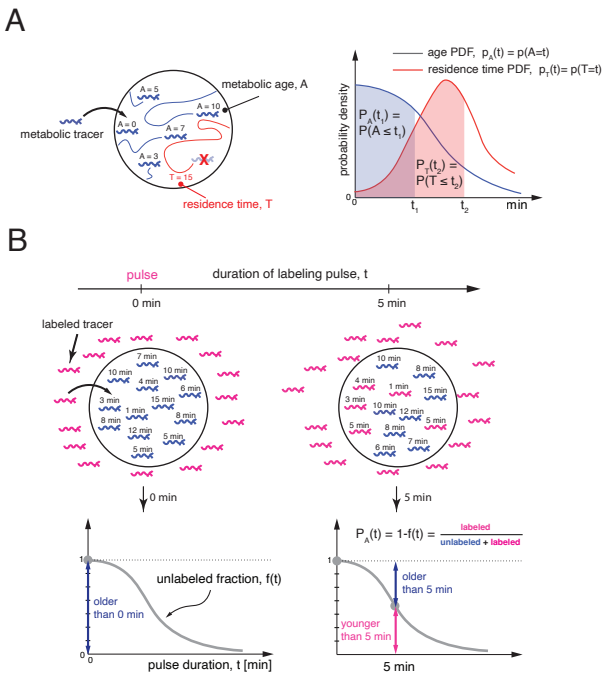

Figure 1: **Equivalence of metabolic age distributions and labeling dynamics.** (A) top: Schematic of a metabolic system (e.g. a cell culture) fed by a metabolic tracer from the external environment. The time elapsed since the tracer entry defines its metabolic age $\mathcal{A}$. Residence time $\mathcal{T}$ is defined as the period between entry and escape. bottom: Example of steady-state distributions of ages and residence times $p_{\mathcal{A}}$ and $p_{\mathcal{T}}$. Shaded ares illustrate the corresponding cumulative probabilities. (B) Renewal of metabolic tracer in cellular pools after the initiation of metabolic labeling ($t = 0$), wherein the unlabeled tracer (blue) is replaced with an isotopically labeled one (pink). Graphs below show the dynamics of the unlabeled fraction in the measured pools, $1-f(t)$, which is equivalent to the metabolic age CDF.

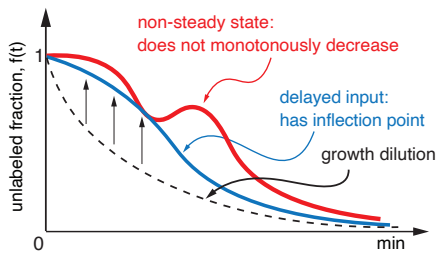

Figure 2: **Criteria of non-steady-state dynamics and delayed input.** Non-monotonous labeling dynamics indicates that the system is not in steady state. A non-convex labeling curve or slower than growth dilution labeling are the signs of delayed input.

4.3 Other dynamic parameters are directly related to labeling dynamics when labeling is not delayed

We can also show that the labeling dynamics defines other dynamic parameters, but only when the tracer can be observed immediately after entry from the external environment, i.e., when the labeling is not delayed

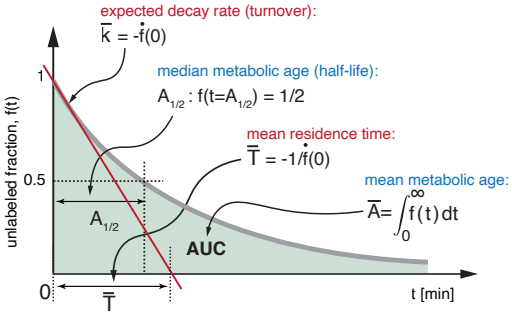

Figure 3: **Cumulative dynamic parameters and their relation to the geometry of the labeling curve in nongrowing systems.** The half-life, $t_{1/2}$, corresponds to the median metabolic age of the measured metabolite. The mean metabolic age, $\bar{\mathcal{A}}$, corresponds to the area under the labeling curve (AUC). The expected decay rates, $\bar{\kappa}$, are defined by the magnitude of the slope of the curve at time 0 and correspond to the tangent to the curve at the initial point (red line). The mean residence time, $\bar{\mathcal{T}}$, corresponds to the point where this tangent intersects with the time axes.

(we show how one can deal with delayed inputs later in Section 4.6). For example, labeled glucose can be detected in the entire cell reasonably immediately when it crosses the cell membrane.

To envision these connections, we avoid specific assumptions about any particularities of internal metabolism by thinking of the metabolic system as a "black box", which allows tracer particles to enter and leave (Figure 4).

Consider that in the absence of delay, all particles entering the system also have an age $\mathcal{A} = 0$ at the time of entry. If we focus on a small batch of "newborn" particles that just entered (within a short time interval dt), the initial relative size of this batch can be quantified using the PDF of age as $p_{\mathcal{A}}(0)dt$. At some later time point t the age of the remaining batch members would be equal to t while the relative batch size would decrease, as some particles have left the system, and correspond to $p_{\mathcal{A}}(t)dt$. Importantly, the missing particles were those that left the system before the time point t. In other words, the decrease in batch size, $p_{\mathcal{A}}(0)dt - p_{\mathcal{A}}(t)dt$, represents those members that had a residence time shorter than t. This allows us to determine the residence time CDF, $P_{\mathcal{T}}(t)$, as the fraction of the initial batch that left the system using the age PDF, as shown in Figure 4A:

$$P_{\mathcal{T}}(t) = \frac{p_{\mathcal{A}}(0) - p_{\mathcal{A}}(t)}{p_{\mathcal{A}}(0)} = 1 - \frac{p_{\mathcal{A}}(t)}{p_{\mathcal{A}}(0)} \tag{5}$$

Taking the derivative (similar to Equation 1) and replacing the age PDF with the labeling dynamics (based on Equation 3), we can get:

$$p_{\mathcal{T}}(t) = -\frac{\dot{p}_{\mathcal{A}}(t)}{p_{\mathcal{A}}(0)} = -\frac{\ddot{f}(t)}{\dot{f}(0)} \tag{6}$$

Therefore, the distribution of residence time, similar to age, can be directly inferred from the labeling dynamics. However, since it depends on the second time derivative,

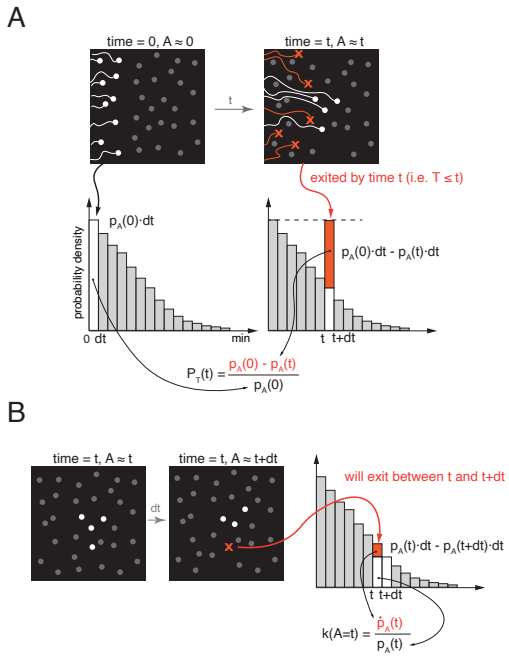

Figure 4: **Metabolic age and residence time distributions are directly related in steady-state metabolic systems.** "Black-box" representation of a steady-state metabolic system that allows tracer particles (white) to enter and leave. Histograms illustrate the distribution of metabolic ages and its relationship to (A) the CDF of residence times or (B) the age-dependent decay rate $\kappa(\mathcal{A})$.

it is likely to be sensitive even to small measurement errors. In fact, Equation 6 also defines a criterion for non-delayed labeling. Since the residence time PDF is always positive and $\dot{f}(t)$ is always negative (Equation 3), $\ddot{f}(t)$ must always be positive, which means that the nondelayed labeling curve must have a convex shape (Figure 2).

Next, we can see that decay rates, i.e. the fractional rates at which particles leave the system, generally depend on their metabolic age. We define the age-dependent decay rate $\kappa(\mathcal{A})$ as the rate at which particles of metabolic age $\mathcal{A}$ leave the system. We again focus on a batch of particles of a certain age, $p_{\mathcal{A}}(t)dt$. A short time later, $t+dt$, a fraction of this batch leaves (decays), while the remaining members age by dt. Therefore, the size of the aged batch can be found as $p_{\mathcal{A}}(t+dt)dt$ (Figure 4B). The decay rate can thus be also directly related to the labeling dynamics as:

$$\kappa(\mathcal{A}) \approx \frac{p_{\mathcal{A}}(t) - p_{\mathcal{A}}(t+dt)}{p_{\mathcal{A}}(t)} \xrightarrow{dt \to 0} -\frac{\dot{p}_{\mathcal{A}}(t)}{p_{\mathcal{A}}(t)} = -\frac{\ddot{f}(t)}{\dot{f}(t)}\,. \tag{7}$$

Specifically, this shows that, in the general case, decay rates cannot be defined by a single value and, similarly to residence times, depend on its first and second time derivatives. One common exception is when the labeling dynamics is characterized by single-exponential decay $f(t) = \mathrm{e}^{-\lambda t}$, in which case $\kappa = \lambda$. However, even in a system consisting of just two separate pools, each with its own constant decay rate, the decay rate in the whole system would be age dependent (Appendix S1.6.1 and

Figure S3A).

Another implication is that the mean values of the decay rate or residence time are defined by the initial slope of the labeling curve (Figure 3, see Appendix S1.3.2-S1.3.3 for the derivations):

$$\begin{aligned} &\text{mean residence time} \quad \bar{\mathcal{T}} \equiv \mathbb{E}[\mathcal{T}] = -\frac{1}{\dot{f}(0)} \\ &\text{expected decay rate} \quad \bar{\kappa} \equiv \mathbb{E}[\kappa(\mathcal{A})] = -\dot{f}(0)\,. \end{aligned} \tag{8}$$

As a consequence, these cumulative stability parameters are generally not related to the overall shape of the labeling curve (Appendix S1.6.1 and Figure S5A) and their experimental determination requires measurements of changes in labeling (the initial slope of the labeling curve) at very short time intervals after the labeling pulse (Appendix S1.8.3). Yet, expected decay rates and mean residence times can also be characterized in a conditional manner that does not require immediate measurements(see Appendix S1.3.7).

Together, unlike metabolic age, the determination of residence times and decay rates using dynamic labeling is highly sensitive to measurement errors and relies on the assumption of immediate labeling.

4.4 Exponential growth affects the connection between labeling dynamics and dynamic parameters

Up to this point, we assumed that metabolic systems have a constant size albeit many experiments are done in growing cell cultures, i.e., when the biomass (or volume) of the whole system increases over time. If the composition of the culture remains uniform and the culture grows exponentially, all its different pools also grow exponentially at exactly the same rate, a condition called *balanced growth*. In this case for every unit volume within the system, the pool composition and the flux magnitudes remain constant, and we can treat such constant volumes mathematically as if they were in steady state.

Since the labeling and age distributions are both defined as fractions relative to all particles in the system, the relationship between these two functions will remain unchanged and follow Equations 1-4, except that the growth rate μ imposes additional constraints on the labeling and mean age (as shown in Appendix S1.3.5):

$$\begin{aligned} f(t) = 1 - P_{\mathcal{A}}(t) \leq \mathrm{e}^{-\mu t} \\ \bar{\mathcal{A}} \leq \mu^{-1} \end{aligned} \tag{9}$$

However, growth does affect the relationships between labeling dynamics and residence times as well as decay rates. Consider a fixed volume of the growing system (which remains V_0, as in Figure 5). All particles entering this fixed volume at $t = 0$ will eventually escape in one of two ways: by decaying or by moving outside and contributing to the growth of the system. The former is quantified as before by $\kappa(\mathcal{A})$, while the latter (which we call growth dilution) is equal to μ, as it must keep the wider system in balanced growth. The two rates are mutually exclusive and, therefore, the *total escape rate* $\lambda(\mathcal{A})$ is given by their sum. On the flip side, $\lambda(\mathcal{A})$ still follows the relation to the age distribution and labeling dynamics in the fixed-volume system, i.e. as in Equation 7. Therefore, we can write:

$$\kappa(\mathcal{A}) = \lambda(\mathcal{A}) - \mu = -\frac{\ddot{f}(t)}{\dot{f}(t)} - \mu\,. \tag{10}$$

Residence times are affected by growth in an even more complex way. Consider a *whole system* having volume V_0 when observed at a certain time point $t = 0$ and that expands at a growth rate μ (Figure 5). As before, a batch of particles that enters this volume at time $t = 0$, can be quantified as $V_0 p_{\mathcal{A}}(0)dt$. However, after some time t, the volume of the system will increase as $V(t) = V_0 e^{\mu t}$ and the remaining batch will have size $V(t)p_{\mathcal{A}}(t)dt$ (Figure 5). The CDF of residence time, by definition, will be equal to the relative fraction of the remaining batch out of the initial size:

$$P_{\mathcal{T}}(t) = \frac{\cancel{V_0} p_{\mathcal{A}}(0)dt - \cancel{V_0}\mathrm{e}^{\mu t} p_{\mathcal{A}}(t)dt}{\cancel{V_0} p_{\mathcal{A}}(0)dt} \tag{11}$$

and we can also get the relationship between the residence time PDF and the labeling by taking the time derivative and replacing $p_{\mathcal{A}}(t)$ with $\dot{f}(t)$:

$$p_{\mathcal{T}}(t) = -\mathrm{e}^{\mu t}\,\frac{\ddot{f}(t) + \mu \dot{f}(t)}{\dot{f}(0)}\,. \tag{12}$$

In summary, balanced growth affects the relation of observed labling dynamics with dynamic parameters. Its effect varies, and the correction required can be either none (for the ages), a simple growth rate subtraction (for the decay rates), or a more complicated expression (for the residence times). For example, as a consequence of growth, the expected decay rate and the mean residence time are no longer inversely related (see Appendix S1.3.4, Equations S16-S17, and Figure S3B).

4.5 Determination of dynamic parameters requires compensation for labeling delay

When linking between the labeling dynamics and dynamic parameters of the observed system, we assumed that the age of particles entering the observed system is $\mathcal{A} = 0$ at the moment of entry, i.e., the labeling is immediate. However, this condition is rarely met in practice as the tracer typically takes some time to reach the observed pools, resulting in delayed labeling. For example, labeling of proteins with stable amino acid isotopomers can be significantly delayed in animal tissues when the tracer is introduced as a dietary supplement [17, 20]. Delays have a clear signature, such as a flat initial slope – $\dot{f}(0) = 0$, areas of nonconvexity – $\ddot{f}(t) < 0$, delayed labeling dynamics of multiply labeled species, and, in case the system is growing, a labeling dynamics which initially is slower than the growth dilution – $f(t) > e^{-\mu t}$ (see Appendices S1.3.5 and S1.4 for derivations, as well as Figure 2).

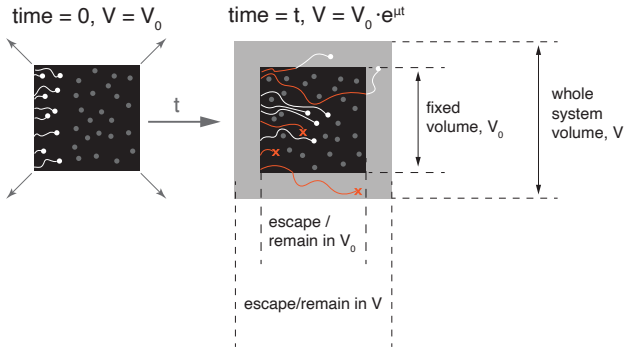

Figure 5: **Dynamics of exponentially growing metabolic systems.** Time-evolution of an exponentially growing dynamic system. After time t since the initial time point, the entire system expands from V_0 by a factor of $e^{\mu t}$. During this time, only some the tracer particles that entered at $t = 0$ would remain in the volume equivalent to V_0 (black box, white dots). The rest would either decay (red crosses) or still remain the entire expanded system (white dots in the gray frame).

Although the effect of delay on the relationship between the dynamic parameters and the observed labeling is not always trivial, we can define a compensation procedure that reduces the entry ages of the tracer particles to $\mathcal{A} = 0$. The labeling dynamics compensated for the delay can then be used to determine all dynamic parameters as described in previous chapters. This can be exemplified with a scenario in which an observed subsystem is fed by a *well-mixed* source (i.e., the fate of particles entering the system is independent of their history) with some known age distribution $p_{\mathcal{A}^\circ}(t)$ (Figure 6A). This scenario is a reasonable description, for example, of cases such as metabolic labeling of RNA or proteins by externally added small-molecule precursors. The age $\mathcal{A}$ of each tracer particle in this case represents a sum of the age at which it entered the observed system, $\mathcal{A}^\circ$, and the time it spent in it from the moment of entry, which we denote by $\mathcal{A}_r$. The $\mathcal{A}_r$ can also be thought of as the age of the particles in an equivalent *reduced* system into which the tracer enters without delay (Figure 6A).

Since $\mathcal{A}^\circ$ and $\mathcal{A}_r$ are independent variables, the probability distribution of their sum is given by a convolution of the two PDFs:

$$p_{\mathcal{A}}(t) = p_{\mathcal{A}^\circ + \mathcal{A}_r}(t) = p_{\mathcal{A}^\circ}(t) * p_{\mathcal{A}_r}(t) \tag{13}$$

where $*$ stands for convolution, i.e., $(g * h)(t) \equiv \int_0^t g(\tau)h(t-\tau)d\tau$. It can also be shown (Appendix S1.7) that the observed labeling dynamics is connected to those in the input and in the reduced system as:

$$f(t) = f^\circ(t) - (\dot{f}^\circ * f_r)(t)\,. \tag{14}$$

As a consequence, when labeling is delayed, the observed labeling dynamics itself is not sufficient to determine the dynamic parameters of the observed system, even if it is known precisely (see Appendix S1.4.3). However, knowing both the observed labeling $f(t)$ and the labeling dynamics of the input $f^\circ(t)$ enables us to determine all of them. For example, one can determine the reduced mean age simply by subtracting the mean age of the input from the observed mean age (see Appendix S1.7):

$$\bar{\mathcal{A}}_r = \bar{\mathcal{A}} - \bar{\mathcal{A}}^\circ\,. \tag{15}$$

or, equivalently, by calculating the area between the curves of $f^\circ(t)$ and $f(t)$ (Figure 6B, see Equation 4). More generally, to determine all the distributions of dynamic parameters, $f_r(t)$ can be found by fitting, based on the convolution relation using Equation 14. In the following sections, we describe the general implementation of the compensation procedure using compartmental models.

In summary, quantification of the dynamic parameters in case of delayed labeling can be achieved when it is possible to define a compensation procedure that reduces the age of metabolic tracer particles upon entry to zero.

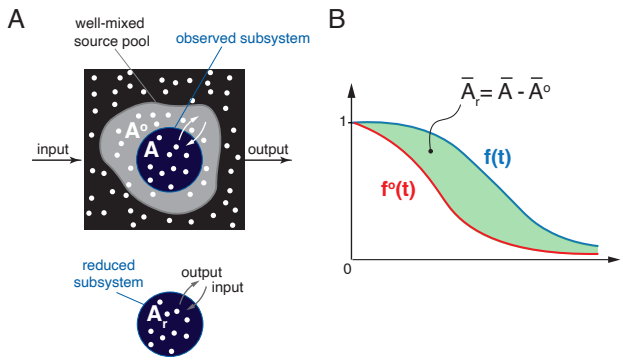

Figure 6: **Determining dynamic properties of systems with delayed input.** (A) Example of a system with delayed input. (top) The observed subsystem (blue) is a part of a larger system and receives some particles from unobserved parts which represent a well-mixed source with a known metabolic age distribution $\mathcal{A}^\circ$. (bottom) Compensating for the input delay is equivalent to resetting the ages of all particles entering the observed subsystem to $\mathcal{A} = 0$, i.e. as if it were connected directly to an external input. The distribution of reduced metabolic ages $\mathcal{A}_r$ reflects the time spent by the tracer in the observed subsystem. (B) Mean reduced age $\bar{\mathcal{A}}_r$ of the tracer can be deduced from the observed labeling dynamics $f(t)$ and labeling dynamics of the input $f^\circ(t)$ as area between the two curves.

4.6 Connecting labeling dynamics with dynamic parameters using compartmental models

The models described so far are non-parametric and do not require any assumptions about the internal structure of the metabolic systems. However, practical quantification of dynamic parameters using these models requires a high sampling frequency and is highly sensitive to measurement noise. As an alternative, one can explicitly represent the internal structure of the metabolic system using a model comprising a set of pools (compartments) connected in a pairwise fashion by fluxes that represent the transfer of material – denoted a *compartmental model* or CM in short and frequently used

in pharmacokinetic analysis [8]. The word *compartmental* is used here in a wide context and can represent not only physical compartments, but also metabolic states and any other type of physical or chemical separation attribute. For example, these can be a set of membrane-delimited organelles connected by molecular transport routes, or metabolites in a pathway connected by enzyme-catalyzed chemical reactions (Figure 7).

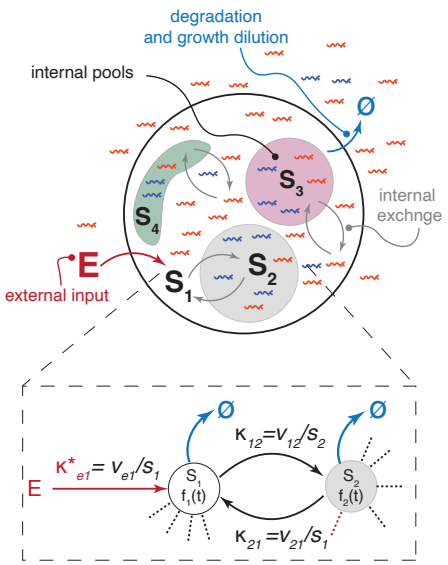

Figure 7: **Description of steady-state labeling dynamics in metabolic systems using compartmental models.** Parametric description of tracer propagation through internal metabolic pools via contributed turnovers that represent connecting flux rates from source to recipient pools in units of the recipient pool size.

Mathematically, CM-based description of metabolic dynamics can be seen as a Markov process in which the possible fates of each particle depend only on its current state and not on its history [28]. For example, in a CM representation of glycolysis, we require that the fate of cytosolic glucose-6-phosphate does not depend on how or when it was imported into the cell. Since this is arguably a fair assumption for any biochemical process, CMs (with an unlimited number of compartments and flux routs) should be able to recapitulate any valid age distribution of a metabolic tracer.

In steady state, the number of compartments (pools) in CMs and their sizes are constant (denoted s_i), and so are the rates of material transfer between pools, κ_{ji}. For a convenient description of dynamic labeling we define transfer rates by the *contributed turnovers* $\kappa_{ji} \equiv v_{ji}/s_i$ and $\kappa_{ei} \equiv v_{ei}/s_i$ that represent influxes from the internal and external pools, respectively, normalized by the size of the receiving pool (Figure 7).

Defining $\mathbf{f}(t)$ as the vector of labeling dynamics across all states and using the above conventions, one can easily see that $\mathbf{f}(t)$ relates to its time derivative via a linear relationship:

$$\dot{\mathbf{f}}(t) = \mathbf{M}\mathbf{f}(t)\,, \tag{16}$$

where $\mathbf{M}$ is referred to as the *state transition matrix* and comprises combinations of contributed turnovers (Figure S1E, see Appendix S1.5.2).

Equation 16 is a first-order linear homogeneous ODE (standard for continuous-time Markov processes [28]) with a known analytical solution [5, 45]:

$$\mathbf{f}(t) \;=\; \mathrm{e}^{\mathbf{M}t}\mathbf{1}_n \tag{17}$$

where $\mathrm{e}^{\mathbf{M}t}$ is a matrix exponential that can be computed numerically [1]. Using this solution, we can define the *system unlabeled fraction* as:

$$f_{\mathbf{s}}(t) \equiv \mathbf{s}^\top \mathbf{f}(t) = \mathbf{s}^\top \mathrm{e}^{\mathbf{M}t}\mathbf{1}_n, \tag{18}$$

where $\mathbf{s}$ is the vector of the relative pool sizes (which sums up to 1). The distributions of metabolic ages, residence times and decay rates, in the metabolic system, as well as their mean/expected values, can then be found using Equations 2-8 (see Appendix S1.5.5 and Table S3 for yet more derivations). For example:

$$\begin{aligned} p_{\mathcal{A}_{\mathbf{s}}}(t) &= -\dot{f}_{\mathbf{s}}(t) = -\mathbf{s}^\top \mathbf{M}\mathrm{e}^{\mathbf{M}t}\mathbf{1}_n \\ \bar{\mathcal{A}}_{\mathbf{s}} = \bar{\mathcal{T}}^* &= \int_0^\infty f_{\mathbf{s}}(t)dt = -\mathbf{s}^\top \mathbf{M}^{-1}\mathbf{1}_n \\ \bar{\mathcal{T}} &= -1/\dot{f}_{\mathbf{s}}(0) = -1/\mathbf{s}^\top \mathbf{M}\mathbf{1}_n \\ \bar{\kappa} &= -\dot{f}_{\mathbf{s}}(0) = -\mathbf{s}^\top \mathbf{M}\mathbf{1}_n\,. \end{aligned} \tag{19}$$

These relationships can also be demonstrated directly (Appendix S1.5.1). Defining $\mathbf{p}_{\mathcal{A}}(t)$ as the vector of all age PDFs, across all states, we can derive a similar to the case of the labeling dynamics relationship (Equation 18):

$$\dot{\mathbf{p}}_{\mathcal{A}}(t) \;=\; \mathbf{M}\;\mathbf{p}_{\mathcal{A}}(t)\,. \tag{20}$$

This directly provides a general analytical solution for the metabolic age distributions for every pool of the metabolic system:

$$\mathbf{1}_n - \mathbf{P}_{\mathcal{A}}(t) \;=\; \mathrm{e}^{\mathbf{M}t}\mathbf{1}_n\,. \tag{21}$$

Since CMs can recapitulate, arguably any valid dynamics of a metabolic system, they can be used both to test hypotheses about their structure and to realistically fit otherwise discrete and noisy experimental data in order to extract dynamic parameters of analyzed systems. In both cases, the experimental data ($\mathbf{f}(t_i)$ values measured at multiple time points – $\{t_i\}$ – and for one or more combinations of internal pools) can be fitted with, for example, a non-linear least-squares solver [8] (Appendix S1.8.1).

Specifically, modeling of delayed labeling scenarios with CMs provides a powerful way to compensate for the labeling delay (see Chapter 4.5). It can be easily seen that if the entire system, including both the observed and unobserved parts, is represented by a CM, the observed system whose labeling is delayed can always be reduced to the equivalent directly labeled system simply by removing all rows and columns from the original $\mathbf{M}$ matrix that describe the unobserved pools and renormalizing the remaining observed pool weights (see Appendix S1.5.3 for further details). The reduced CM denoted by $\mathbf{M}_r$ and $\mathbf{s}_r$ can then be used to determine the dynamic parameters of the observed system as if it were labeled without delay, which we illustrate using practical examples in Chapter 4.8.

4.7 Properties of labeling dynamics related to compartmental models

The CM representation defines what labeling curves can and cannot look like. One general property, which is a consequence of the general solution for the labeling dynamics from Equation 16, is that any real labeling dynamics can be represented as the sum of exponents, namely $\sum_i e^{\lambda_i t}$ where λ_i are the eigenvalues of $\mathbf{M}$ all of which have negative real part. In turn, $\mathbf{M}$ must satisfy the requirement of mass balance in which every part of the metabolic system receives as much material as it lets out. This *mass balance constraint* can be formed as:

$$\mathbf{M}^\top \mathbf{s} \leq -\mu \mathbf{s}, \tag{22}$$

where μ is the growth rate and can be 0 in the case of non-growing systems (Appendix S1.5.2). One can show (see Lemma S1.17) that given $\mathbf{M}$ and μ, there exists a pool size vector $\mathbf{s}$ that satisfies the mass balance constraints if and only if all real parts of the eigenvalues of $\mathbf{M}$ are smaller than $-\mu$. As a consequence, for sufficiently long timescales the values of $\mathbf{f}(t)$ always decrease exponentially and faster than the growth rate (Appendix S1.5.4). This makes intuitive sense, since if one or more eigenvalues were larger (less negative), the solution would include an exponent that decays more slowly than μ, and would therefore be inconsistent with balanced growth.

4.8 Example 1: quantifying dynamics of yeast proteome in mild heat stress

To illustrate the practical application of our age-based framework and CMs, we used it to determine the metabolic age of budding yeast proteins and to detect proteins with complex decay patterns at normal growth temperature and under mild heat stress conditions. Using $^{13}C_6^{15}N_2$-L-lysine, we pulse-labeled yeast cultures maintained in a balanced growth regime at 30°C (optimal temperature) or 37°C (mild heat stress) and analyzed protein labeling (i.e., the fraction of unlabeled lysine in each protein) by quantitative mass spectrometry over a period of approximately three doubling times (Figure 8A and Figures S6A). As expected, the culture grown at 37°C showed an elevated abundance of heat shock proteins, which confirms the adaptation to heat stress (Figure S6B).

We first asked whether there was a substantial delay in the labeling of proteins, e.g., due to a stockpile of free cationic amino acids [9, 32]. Indeed, we found that under both conditions the cumulative protein labeling curves (all peptides combined) showed two indicators of a strong delay in labeling – an inflection point at around one doubling time and values that are significantly above the growth dilution limit of the cultures (Figures 2 and 8B). In further support, free lysine in yeast cells was labeled relatively slowly at both temperatures (Figure 8B).

Assuming that the fate of lysine incorporated into proteins is independent of its previous history (i.e., a "well-mixed" labeling scenario, see Chapter 4.5), compensation for the labeling delay can be achieved knowing the

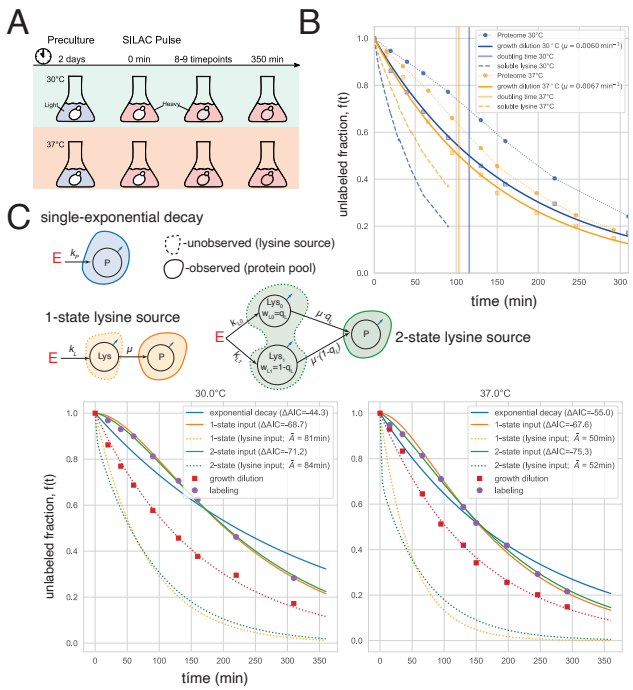

Figure 8: **Quantification of protein labeling delay in dynamic labeling assays with stable heavy lysine isotopomer.** (A) Schematic of dynamic labeling assay. (B) Labeling dynamics of the whole proteome (thin dashed) quantified at 30°C (blue) and 37°C (gold) based on all peptide intensities combined as compared to the growth dilution dynamics of the same culture (solid) and to directly measured labeling dynamics of free lysine in similar labeling conditions (thick dashed). Vertical colored lines - culture doubling times at 30°C (blue) and 37°C (gold). (C) (top) CMs representing direct lysine input (single-exponential decay), 1-state lysine input and 2-state lysine input and used to fit labeling dynamics of reference proteins. Color and dash patterns correspond the fitted labeling dynamics of lysine input, *Lys*, and of reference proteins, *P*. κ - contributed turnovers; w - pool weights; μ - culture growth rate. (bottom) Labeling dynamics of lysine in the input (dashed) and in the reference protein pool (solid) calculated by fitting the CM variants with the median labeling values of reference proteins (purple dots). ΔAIC and $\bar{\mathcal{A}}$ measure the quality of CM fits (the lower the better) and the mean age of lysine input, respectively.

labeling dynamics of lysine used for protein synthesis $f^\circ(t)$ (Equation 14). The direct measurement of $f^\circ(t)$ is not straightforward, but it can be determined indirectly using reference proteins, defined as the proteins with the highest mean age in the growing system and whose labeling curve is therefore closest to the growth dilution limit, namely $\approx e^{-\mu t}$ (see Equation 9). The $f^\circ(t)$ can then be calculated using the labeling dynamics of these proteins to fit a CM in which they represent a growth-diluted pool and are fed by an unknown lysine source (Figure 8C).

To identify reference proteins, we evaluated the mean metabolic age of lysine in each protein by modeling their labeling dynamics with a 2-state CM in which the labeling delay is generated by a single unobserved pool

Description [dimension]	Symbol	Expression of $\mathcal{A}$	Expression of f	Expression of M, s
unlabeled fractions [unitless]	$\mathbf{f}(t)$	$\mathbf{1}_n - \mathbf{P}_{\mathcal{A}}(t)$	$\mathbf{f}(t)$	$\mathrm{e}^{\mathbf{M}t}\mathbf{1}_n$
metabolic ages PDF [time^{-1}]	$\mathbf{p}_{\mathcal{A}}(t)$	$\mathbf{p}_{\mathcal{A}}(t)$	$-\dot{\mathbf{f}}(t)$	$-\mathbf{M}\mathrm{e}^{\mathbf{M}t}\mathbf{1}_n$
mean ages [time]	$\bar{\mathcal{A}}$	$\int_0^\infty t\,\mathbf{p}_{\mathcal{A}}(t)\,dt$	$\int_0^\infty \mathbf{f}(t)dt$	$-\mathbf{M}^{-1}\mathbf{1}_n$
system unlabeled fraction [unitless]	$f_{\mathbf{s}}(t)$	$1 - P_{\mathcal{A}_{\mathbf{s}}}(t)$	$\mathbf{s}^\top\mathbf{f}(t)$	$\mathbf{s}^\top\mathrm{e}^{\mathbf{M}t}\mathbf{1}_n$
system age PDF [time^{-1}]	$p_{\mathcal{A}_{\mathbf{s}}}(t)$	$p_{\mathcal{A}_{\mathbf{s}}}(t)$	$-\dot{f}_{\mathbf{s}}(t)$	$-\mathbf{s}^\top\mathbf{M}\mathrm{e}^{\mathbf{M}t}\mathbf{1}_n$
mean system age [time]	$\bar{\mathcal{A}}_{\mathbf{s}}$	$\int_0^\infty t\,p_{\mathcal{A}_{\mathbf{s}}}(t)\,dt$	$\int_0^\infty f_{\mathbf{s}}(t)dt$	$-\mathbf{s}^\top\mathbf{M}^{-1}\mathbf{1}_n$
median system age (half-life) [time]	$t_{\mathbf{s},1/2}$	$P^{-1}_{\mathcal{A}_{\mathbf{s}}}\left(\frac{1}{2}\right)$	$f^{-1}_{\mathbf{s}}\left(\frac{1}{2}\right)$	t s.t. $\mathbf{s}^\top\mathrm{e}^{\mathbf{M}t}\mathbf{1}_n = \frac{1}{2}$
system residence time PDF [time^{-1}]	$p_{\mathcal{T}}(t)$	$-\dot{p}_{\mathcal{A}_{\mathbf{s}}}(t)/p_{\mathcal{A}_{\mathbf{s}}}(0)$	$-\ddot{f}_{\mathbf{s}}(t)/\dot{f}_{\mathbf{s}}(0)$	$-\mathbf{s}^\top\mathbf{M}^2\mathrm{e}^{\mathbf{M}t}\mathbf{1}_n \,/\, \mathbf{s}^\top\mathbf{M}\mathbf{1}_n$
mean system residence time [time]	$\bar{\mathcal{T}}$	$-1/p_{\mathcal{A}_{\mathbf{s}}}(0)$	$-1/\dot{f}_{\mathbf{s}}(0)$	$-1 \,/\, \mathbf{s}^\top\mathbf{M}\mathbf{1}_n$
system decay rate [time^{-1}]	$\kappa(\mathcal{A}_{\mathbf{s}})$	$-\dot{p}_{\mathcal{A}_{\mathbf{s}}}(t)/p_{\mathcal{A}_{\mathbf{s}}}(t)$	$-\ddot{f}_{\mathbf{s}}(t)/\dot{f}_{\mathbf{s}}(t)$	$-\mathbf{s}^\top\mathbf{M}^2\mathrm{e}^{\mathbf{M}t}\mathbf{1}_n \,/\, \mathbf{s}^\top\mathbf{M}\mathrm{e}^{\mathbf{M}t}\mathbf{1}_n$
system decay rate [time^{-1}]	$\bar{\kappa}$	$p_{\mathcal{A}_{\mathbf{s}}}(0)$	$-\dot{f}_{\mathbf{s}}(0)$	$-\mathbf{s}^\top\mathbf{M}\mathbf{1}_n$

Table 1: **Dynamic parameters of steady-state systems and their relation to the metabolic age, experimental labeling dynamics, and compartmental model parameters.** The expressions connecting labeling dynamics, age distributions, and residence times with CM parameters. Some of these can be defined for each individual state, and also for the whole system (i.e. the weighted average across all the pools, in proportion to their sizes). For a more comprehensive summary, see Table S3.

(Figure S6C). As during well-mixed labeling the effect of this delay is the same for all proteins (Equation 15), we identified the reference proteins by calculating the mean metabolic ages of lysine based on the CM fit using Equation 4 and selecting the ones with the highest mean age (Figure S6C-D). We could then determine $f^\circ(t)$ by testing different lysine inputs to explain this labeling dynamics and selecting the best model based on Akaike's information criterion (AIC). At both temperatures, $f^\circ(t)$ was best described by two parallel pools (fast and slow) that also produce a significantly different labeling delay at 30°C and 37°C, corresponding to the mean age of lysine input of ≈80 min and ≈50 min, respectively (Figure 8C).

Knowing $f^\circ(t)$, in turn, allowed us to quantify the dynamic parameters of all proteins at both temperatures using a similar CM-based approach. We first modeled the dynamics of lysine labeling in each protein as if it were an observed subsystem with unknown parameters fed by the known lysine source (Figure 9A). The parametrized CM and the CM reduction approach (Chapter 4.6) were then used to calculate $f_r(t)$ and convert it to the dynamic parameters. Since our time course included relatively few measurements, we used only the simplest single-pool or two-pool options to represent proteins, selecting the best according to AIC (Figure 9A). The two-pool model was used specifically to identify proteins that have complex (age-dependent) decay patterns (see Example S1.6.1). Based on the AIC score, only a small fraction of the proteins (≈10% in 30°C and ≈6% in 37°C) required a more complex two-pool model to explain their labeling dynamics (Figure 9A).

Since residence times and decay rates (unlike ages) depend on the first and second time derivatives of the labeling dynamics (see Chapters 4.3), these parameters might be hard to determine accurately in such experiments due to the requirement of high measurement frequency and a high sensitivity to measurement noise. Indeed, our quantification of mean residence times and expected decay rates was much more sensitive to the type of CM used compared to mean ages (the mean fractional difference between the models was at least 30 times higher for residence time and expected decay rate compared to mean age) (Figure S7A and B) supporting the notion that unlike residence times or decay rates, metabolic ages are robustly quantifiable with dynamic labeling.

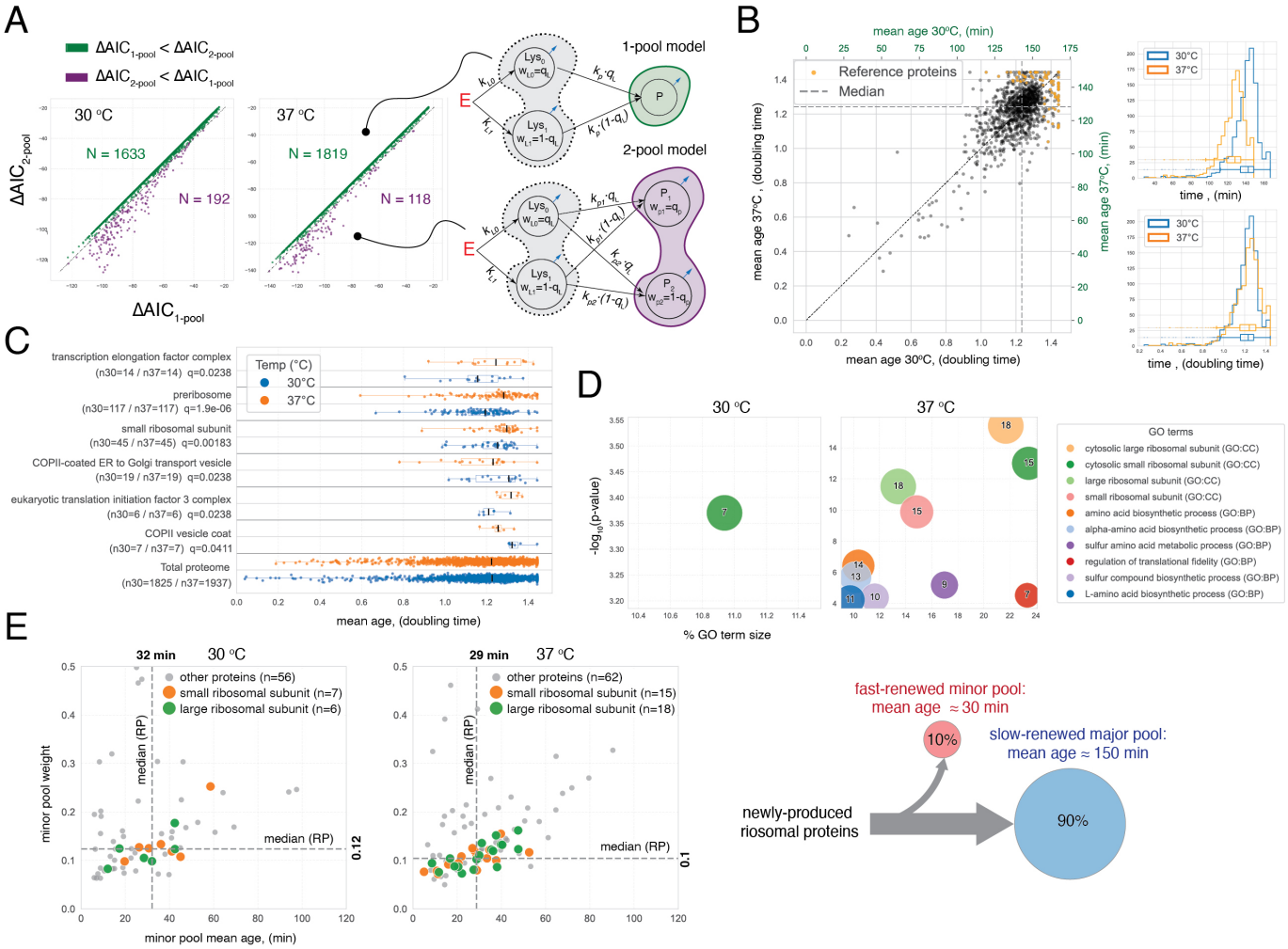

Figure 9: **Comparison of dynamic parameters of yeast proteome at 30°C and 37°C.** (A) Labeling dynamics of yeast proteins at 30°C and 37°C described by one or two protein pools (1-pool and 2-pool models, respectively). Note that for the majority of proteins a single pool model is sufficient to describe labeling dynamics. (B)Comparison of mean metabolic ages of proteins at 30°C and 37°C. Note that conversion of metabolic ages to units of doubling time (right histograms) eliminates systematic differences between temperatures. (C) Protein groups classified based GO annotation with significantly different mean metabolic ages as judged by a two-sided paired t-test and controlled for false discovery rate using Benjamini-Hochberg procedure. For proteins within each group the mean metabolic ages expressed in units of doubling time were plotted (jittered points), showing medians and interquartile ranges. The total proteome was included as a reference. (D)GO enrichment analysis of proteins in (A) whose labeling dynamics in better described by a 2-pool CM. (E) Dynamic parameters of the minor pool of ribosomal proteins (RP) that are better explained by a two-pool model.

We next compared the mean ages of the same yeast proteins at 30°C and 37°C. At both temperatures, metabolic ages had a rather narrow distribution (IQR ≈ 15 min), but proteins appeared systematically younger at 37° C (median: $\bar{\mathcal{A}}_{r\ 37°\mathrm{C}} \approx 130$ min vs. $\bar{\mathcal{A}}_{r\ 30°\mathrm{C}} \approx 140$ min). Interestingly, this difference was mostly eliminated if the mean ages were quantified in units of cell culture doubling time (median $\bar{\mathcal{A}}_r \approx 1.23$ for both temperatures). With this, metabolic ages of most proteins were within ≈ 5% difference between the temperatures (Figure 9B and Figure S7C), indicating that the main driver of temperature-dependent age differences is the duration of the cell cycle. However, there were some exceptions; for example, many components of the translation machinery appeared older at 37° C, while the opposite was true for COPII-mediated ER export components (Figure 9C and Figure S7E). Importantly, compensation for labeling delay was essential for correct quantification of metabolic ages, as, for example, direct fitting of log-transformed labeling dynamics with a linear model [40] led to overestimation of mean ages beyond the growth dilution limit (Figure S7F).

Notably, most yeast proteins showed mean metabolic ages relatively close to the growth dilution limit $\bar{\mathcal{A}} \approx \mu^{-1}$ (Equation 9 and Figure S7 D), indicating that the bulk observed protein populations do not strongly decay and their ages are determined primarily by growth dilution. To characterize the propensity of steady-state protein populations to decay, we quantified the *characteristic lifespan* $\bar{\mathcal{L}} = (\bar{\mathcal{A}}^{-1} - \mu)^{-1}$, defined as the residence time of a uniformly decaying protein pool with the same mean metabolic age (Appendix S1.3.6). The median $\bar{\mathcal{L}} \approx 15$ h was generally consistent with previously published half-life values of $t_{1/2} \approx 9$ h, which for a homogeneous protein pool would correspond to

$\bar{\mathcal{L}} = t_{1/2} / \ln 2 \approx 13$ h [7] (Figures S7G).

In our analysis, some proteins required a two-pool model to describe their labeling dynamics, indicating the presence of subpopulations with distinct decay patterns(Figure 9A). Interestingly, this category at both temperatures was dominated by structural ribosomal proteins (Figure 9D) where approximately 5−15% of the protein population represented the fast-renewed pool with a mean metabolic age of ≈ 30 min (Figures 9E and S7H). This finding supports the previously proposed existence of fast-degraded ribosomal protein pools [41].

In conclusion, these results illustrate how dynamic labeling and the CM-based framework can be used to quantify the metabolic ages of proteins under different conditions, accounting for biases such as labeling delays, and to detect proteins with complex decay patterns.

4.9 Example 2: determining order and time scale of sequential cellular processes

Dynamic labeling and the metabolic age metric can be especially advantageous to analyze specific types of cellular processes. One such example is sequential processes, known as metabolic chains. Using the CM representation, one can show that in a metabolic chain (a set of consecutive interconversions of metabolites), the upstream metabolic pools are always younger and labeled faster than the downstream ones, that is, at any time $t \geq 0$:

$$f_{i-1}(t) \leq f_i(t)\,, \tag{23}$$

where i is the sequential pool index (see Appendix S1.6.4). This property enables the use of dynamic labeling as a simple way to determine the order of events in such processes.

To illustrate this in practice, we reanalyze the data from Onischenko et al. [33] using our age-based framework to infer the assembly order of the yeast nuclear pore complex (NPC) based on the labeling dynamics of affinity-isolated protein complexes between bait and prey NPC subunits (Figure 10A).

To envision how this bait-prey labeling dynamics is connected to the assembly order, we consider that from the perspective of the traced metabolite (lysine in this case) incorporated into a prey, its fate after entering the cell represents a metabolic chain in which the later the NPC bait joins the NPC prey, the slower the labeling of the co-isolated prey pool would appear. In other words, the order in which the baits co-assemble with a given prey can be inferred by comparing the prey labeling in their affinity-isolated complexes (Figure 10B). If we would focus just on the set of bait subunits, each of them co-isolates all the other baits as prey, and the order in which this set assembled with each other can be recapitulated by knowing all such partial assembly orders based on the labeling values.

To implement this, we first calculated an *age score* (see Figure S8A and Materials and Methods S2.10) which corresponds to the assembly order based on the principles described above. Then, we probed all possible hierarchical assembly models for consistency with these age scores, using Spearman rank correlation for grading them (see Figure S8B and C and Materials and Methods Section S2.11). This showed that high-scoring assembly hierarchies could not be produced randomly while the highest-scoring assembly models were in good agreement with the previously reported three-tier model of NPC assembly [33] (Figure 10C and S8D). Furthermore, this framework appeared resistant to the selection of the baits used for the analysis or the way of calculating age scores showing globally similar top-scoring models and correctly predicting the immediate assembly of directly interacting baits (Figures 10 C and S8E and F). Together, this exemplifies how the age-based interpretation of metabolic labeling and CMs can be used to dissect the order of metabolic events.

The age interpretation also allows for gaining insight into the time scale of cellular processes. We can illustrate this in the same example by evaluating with minimal assumptions the *minimal maturation time* $\bar{T}_{\min}$ required for the NPC subunits to assemble in the mature NPC, marked by latest joining protein, Mlp1, in our assembly model (Figure 10C). To this end, we consider that the metabolic age of lysine $\mathcal{A}$ in preys co-isolated with Mlp1 is the sum of three components:

$$\mathcal{A} = \mathcal{A}^{\circ} + T + \mathcal{A}_{\mathrm{NPC}} \tag{24}$$

where $\mathcal{A}^{\circ}$ is the age of lysine in the input, T is the maturation time of the subunit (i.e., the time required for the newly produced subunit to become part of the mature NPC), and $\mathcal{A}_{\mathrm{NPC}}$ is the reduced age of the subunit in the mature NPC (see Figure 10D). Furthermore, from linearity of expectation, the additive relationship in Equation 24 applies also to the mean values, which can be used to compute the mean maturation time of the subunits as:

$$\bar{T} = \bar{\mathcal{A}} - \bar{\mathcal{A}}^{\circ} - \bar{\mathcal{A}}_{\mathrm{NPC}}\,. \tag{25}$$

Since the reduced mean ages are bound by growth dilution ($\bar{\mathcal{A}}_{\mathrm{NPC}} \leq \mu^{-1}$, see Equation 9), we can derive the constraint on the maturation time:

$$\bar{T} \geq \bar{T}_{\min} \equiv \bar{\mathcal{A}} - \bar{\mathcal{A}}^{\circ} - \mu^{-1}\,. \tag{26}$$

To compute this minimal bound (right side), we determined the mean metabolic age of lysine $\bar{\mathcal{A}}$ using experimental labeling values of the Mlp1 prey with Equation 4 and quantified $\bar{\mathcal{A}}^{\circ}$ based on our previous analysis of lysine labeling delay in these experiments [33] (see Appendix S2.10). This showed that $\bar{T}_{\min}$ for most NPC components was on the order of one hour, in agreement with the slow incorporation of the Mlp1 subunit into NPCs [33, 49] (Figure 10 D). In further support, Nsp1 – a subunit that shows an exceptionally large $\bar{T}_{\min}$ – has previously been reported to have large cytosolic precursor pools prior to incorporation into NPCs [34].

Overall, these results demonstrate the utility of dynamic labeling and the metabolic age metric to determine the order and time scale of sequential cellular processes.

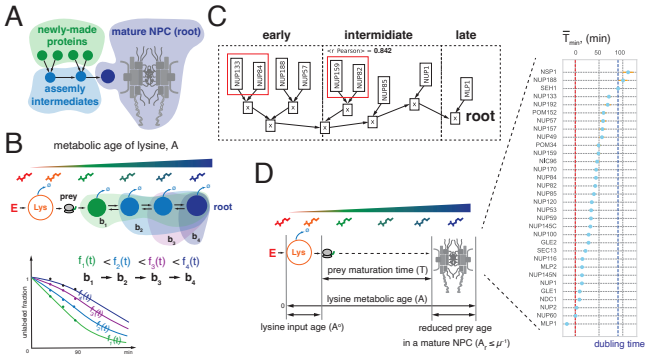

Figure 10: **Determining the order and time scale of NPC assembly using dynamic labeling.** (A) Hierarchical model of NPC assembly (assembly tree): newly-made NPC complements (leafs) first co-assemble into intermediates (branches) which in turn assemble into the mature structure (root). (B) Metabolic path of externally added lysine contained in a prey. The path is a metabolic chain that begins in the external pool (E) and ends in the pool of mature NPC (root). The age of lysine in a prey (colored areas) grows according to the order in which it co-assembles with baits which is reflected by progressively slower labeling dynamics of the prey. (C) Best-scoring assembly model of baits with each other. Red boxes depict known directly interacting proteins. (D) Minimal maturation times of NPC subunits required to assemble into Mlp1-positive NPCs.

5 Discussion

Since the advent of pulse-chase labeling techniques in the 1940s [37, 38], dynamic characteristics of cellular metabolism, e.g., the time a molecule spends in certain parts of the metabolic system or its degradation rate, have been of central importance in understanding cellular homeostasis. In this work, we describe the analysis of steady-state cellular metabolism by dynamic labeling in the most general way. The key to our approach is the equivalence drawn between the experimentally observed labeling dynamics of a tracer and its metabolic age distribution (Chapter 4.2). We use this equivalence to link the readouts of dynamic labeling experiments with various characteristics of metabolic dynamics including age, residence time, and decay rate (Chapters 4.2–4.3).

To establish these connections, we used two alternative approaches to represent metabolic systems: either as a featureless "black box" (Chapter 4.3) or as a compartmental model (CMs) that explicitly describes the metabolic system as a set of compartments and their connecting fluxes (Chapter 4.6). Each of these descriptions has its own advantages. Black-box models are nonparametric and require fewer assumptions. They are widely adopted in geophysics and geochemistry to analyze the dynamics of natural water reservoirs and the atmosphere [3, 15, 16] and can be used to highlight the most basic principles that govern metabolic dynamics. Using the black-box representation we show that dynamic characteristics of metabolic systems can be represented by continuous probability distributions or functions that are in turn encoded in the geometry of the experimental labeling curve (Chapters 4.2–4.3 and Figure 3). This approach was also instrumental in understanding how these connections are distorted by common confounding factors, including cell growth, delayed labeling, or non-steady state metabolic dynamics (Chapters 4.4–4.5), and how these distortions can be detected in the experimental labeling dynamics (Figure 2).

Unlike the black-box representation, CMs mechanistically describe metabolic systems at an arbitrary level of detail by viewing them as a system of well-mixed compartments and their connecting fluxes (Figure 7). Although specific CMs are sometimes used to interpret pulse-chase metabolic labeling experiments [6, 17, 18, 25], our study takes the next step to generalize this description, capitalizing on a relatively well-developed mathematical backbone of CMs, the continuous-time domain Markov processes [28]. In order to demonstrate the strength of this framework, we focus on several useful applications: testing hypotheses about metabolic systems, e.g., which reaction topologies (number of states and their connections) are able to recapitulate the measured data; smoothing out the sparse and noisy experimental labeling dynamics in a physically plausible way; extracting various dynamic parameters such as residence time and decay rate; or compensation for delayed labeling (Sections 4.6–4.9). We demonstrate how using these properties in a systematic way can improve the resolution of dynamic labeling experiments, such as enabling the detection of distinct kinetic pools of analyzed molecules (Figure 9).

CMs can also highlight additional general properties of steady-state labeling dynamics that are not directly evident from black-box models. For example, the labeling curve can always be represented as a sum of exponential decay functions, where the decay coefficients are all bounded by the growth rate (Chapter 4.7). Furthermore, this function is independent of the details of the underlying chemistry, e.g., which reactions have zero-order versus first-order kinetics.

Beyond general descriptions, our analysis has important practical implications. We show that common stability characteristics – residence times, decay rates, and other related parameters – depend on the first and second time derivatives of the labeling dynamics (Chapter 4.3). These interpretations can therefore be highly sensitive to measurement noise and require frequent sampling for accurate quantification. For example, the quantification of cumulative stability characteristics, expected decay rates, and mean residence times depend on the initial labeling dynamics and can be highly biased in the presence of fast-decaying subpopulations, such as reported for some RNA and protein species [11, 26, 39], unless accurate and fast measurements are available (see example in Figure S5A). As a measure less sensitive to these biases, we propose using the *characteristic lifespan*, defined as the mean residence time of equivalent uniformly decaying molecules of the same mean age. As such, the characteristic lifespan can fairly represent the stability of the most abundant molecular pools (Chapter 4.8). Notably, stability characteristics can also be determined using reference-based approaches that do not

suffer from some limitations of dynamic labeling [31, 44].

We also address the issue of delayed labeling, i.e. when the tracer molecules do not immediately enter the observed pool (Chapter 4.5). In such cases, many of the relationships between the dynamic parameters do not hold and could lead to biases such as overestimated residence times (Figure S5B). Therefore, it is necessary to compensate for the delay, e.g. as has been demonstrated in the past and present study for cellular amino acids [6, 17, 18, 25, 33] (Chapter 4.8). However, it is quite often that the delay follows a complex pattern, and these simple compensation methods are insufficient. In this study, we describe an example of NPC maturation in which the labeling dynamics of the same protein can be delayed differently in different subcellular pools, reflecting a progressive increase in metabolic age during the assembly of protein complexes (Figure 10). The latter is an example where the delay itself is a useful feature that can be used to reconstruct a dynamic model for protein complex assembly. In fact, similar effects may provide an alternative explanation for the differences in labeling dynamics frequently observed depending on a subcellular compartment or post-translational modifications of proteins that are regularly attributed to differences in their stability in these distinct pools [2, 19, 25, 43, 46, 47].

The key outcome of our analysis is that metabolic age, that is, the time since the traced metabolite entered the metabolic system, is directly quantifiable in dynamic labeling experiments, while other dynamic parameters require additional assumptions such as direct labeling (Chapter 4.2). Moreover, the cumulative parameters related to age, the mean and median values, are defined by the entire labeling curve (Chapters 4.2 and 4.5) and therefore can be robustly quantified from the experimental labeling dynamics. However, so far, age has not been a common metric of metabolic dynamics. Differences in labeling dynamics were associated with the relative age of different proteoforms [19], while a recent study qualitatively evaluated the age of specific protein pools associated with the proteasome using sequential multiple isotopic labeling [27]. Our study shows the general utility of quantifying the metabolic age based on dynamic labeling to determine the order and time scale of sequential cellular processes and , through this, may shed new light on the interpretation of many dynamic labeling experiments.

Lastly, as part of this study, we developed an open-source Python package to simulate and fit CMs to dynamic labeling data. Although there are publicly available compartmental modeling solutions such as `LAPM` and `CompartmentalSystems` created by Metzler and Sierra [28], our package focuses specifically on the analysis of dynamic labeling experiments and adds unique features that are especially useful for describing metabolic processes in live cells, such as modeling growing systems, introducing mass balance constraints, and flexibly manipulating CMs. Furthermore, it implements non-parametric methods such as the trapezoid integration technique for mean age estimation. We provide several practical examples (Chapters 4.8- 4.9) of implementing the age-based framework to analyze and interpret the results of various dynamic labeling experiments.

6 Materials and methods

Culture conditions, protein labeling and abundance quantification. Dynamic labeling assays were performed using a haploid BY4742 strain (*MATα his3Δ1 leu2Δ0 lys2Δ0 ura3Δ0*) auxotrophic for lysine. Cell cultures were grown at 30°C or 37°C in standard synthetic complete medium containing 6.7 g/L yeast nitrogen base without amino acids and with ammonium sulfate, 2% glucose, necessary amino acids and specifically supplemented at 25 mg/L f.c. with normal [$^{12}C_6$,$^{14}N_2$] L-lysine or heavy [$^{13}C_6$,$^{15}N_2$] L-lysine isotopomer (Silantes), referred to as "light medium" and "heavy medium", respectively. Light-to-heavy-medium exchange for the labeling pulse and sample collection was performed by filtration. The yeast samples were lysed using glass beads and cellular proteins were trypsinized by a standard in-gel digestion protocol. Tryptic peptides were analyzed with Eclipse Tribrid mass spectrometer in DIA mode, and quantified in light and heavy channels using DIA-NN 2.1.0 [10]. The fractional labeling of lysine in the protein pools (the unlabeled fraction) and relative protein abundances were quantified based on the DIA-NN report using a custom Python script available as the Jupyter Notebook (see section on Data and software availability).

Extraction of dynamic parameters using compartmental models. All CM instances used to extract dynamic parameters from labeling data or to simulate labeling curves were implemented with an open source Python package, named `symbolic-compartmental-model`, that we developed as part of this study (see Data and software availability). This package is based on SymPy [29] and provides a list of useful functions to calculate dynamic parameters, including distributions of ages, residence times, and decay rates. In addition, one can use it to determine the cumulative values of these dynamic parameters based on the observed labeling dynamics either numerically or symbolically.

Bioinformatic analysis. Protein abundances were compared between conditions (30° C and 37° C) using the normalized $\log_2$ transformed relative abundance ratio as a metric and a two-sided Welch's t-test for significance determination. All GO term analyses were performed using g:Profiler API [23] calls to acquire annotations and GO term sizes. GO term enrichment was assessed using the g:Profiler API (for 2-pool CM) or by local paired t-tests with Benjamini-Hochberg FDR correction. Gene overlaps with experimental data were computed locally. All bioinformatic analyses were run on a Windows-based workstation.

Detailed description of experimental procedures can be found in the Appendix (Section S2).

Data and software availability. The Python package for CM calculations can be

found in https://gitlab.com/elad.noor/symbolic-compartmental-model. The documentation for this package can be found in https://symbolic-compartmental-model.readthedocs.io/.

All Jupyter notebooks and the accompanying code that were used to analyze the labeling and growth rate data related to heat stress in yeast, as well as the bioinformatic analysis described above, can be found in https://doi.org/10.5281/zenodo.17101594.

Data on protein abundance and dynamic metabolic labeling from previously published works [33] and algorithms used to define the order and timescale of nuclear pore complex based on the metabolic age metric can be found in https://doi.org/10.5281/zenodo.17116706.

7 Acknowledgments and funding sources

We thank Corentin Briat for his generous help in the mathematical proofs related to Metzler matrices, Jonas Fischer, Elisa Dultz and Melody Cools for critically reading and providing useful feedback on the manuscript. Mass spectrometry-based proteomic analyses were performed by the Proteomics Unit at the University of Bergen (PROBE), a member of the National Network of Advanced Proteomics Infrastructure (NAPI) funded by the Research Council of Norway (INFRASTRUKTUR-program project number: 295910). This work was supported by a grant NFR 315615 awarded by the Research Council of Norway to Evgeny Onischenko and Elad Noor.

References

[1] David Betounes. "Linear Systems". en. In: *Differential Equations: Theory and Applications*. Ed. by David Betounes. New York, NY: Springer, 2010, pp. 119–219. ISBN: 978-1-4419-1163-6. DOI: 10.1007/978-1-4419-1163-6_4.

[2] François-Michel Boisvert et al. "A Quantitative Spatial Proteomics Analysis of Proteome Turnover in Human Cells". en. In: *Molecular & Cellular Proteomics* 11.3 (Mar. 2012), p. M111.011429. ISSN: 15359476. DOI: 10.1074/mcp.M111.011429.

[3] Bert Bolin and Henning Rodhe. "A note on the concepts of age distribution and transit time in natural reservoirs". In: *Tell'Us* 25.1 (Feb. 1973). Publisher: Stockholm University Press, pp. 58–62. ISSN: 0804-6042. DOI: 10.1111/j.2153-3490.1973.tb01594.x.

[4] Leon Y. Chan et al. "Non-invasive measurement of mRNA decay reveals translation initiation as the major determinant of mRNA stability". eng. In: *eLife* 7 (Sept. 2018), e32536. ISSN: 2050-084X. DOI: 10.7554/eLife.32536.

[5] Yi Ern Cheah and Jamey D Young. "Isotopically nonstationary metabolic flux analysis (INST-MFA): putting theory into practice". In: *Curr. Opin. Biotechnol.* 54 (Dec. 2018), pp. 80–87. ISSN: 0958-1669. DOI: 10.1016/j.copbio.2018.02.013.

[6] Surendhar Reddy Chepyala et al. "JUMPt: Comprehensive Protein Turnover Modeling of In Vivo Pulse SILAC Data by Ordinary Differential Equations". en. In: *Analytical Chemistry* 93.40 (Oct. 2021), pp. 13495–13504. ISSN: 0003-2700, 1520-6882. DOI: 10.1021/acs.analchem.1c02309.

[7] Romain Christiano et al. "Global proteome turnover analyses of the Yeasts S. cerevisiae and S. pombe". In: *Cell Rep.* 9.5 (Dec. 2014), pp. 1959–1965. ISSN: 2211-1247. DOI: 10.1016/j.celrep.2014.10.065.

[8] Claudio Cobelli, David Foster, and Gianna Toffolo. *Tracer Kinetics in Biomedical Research: From Data to Model*. en. Google-Books-ID: 9tb2BwAAQBAJ. Springer Science & Business Media, May 2007. ISBN: 978-0-306-46833-9.

[9] Melody Cools et al. "Nitrogen coordinated import and export of arginine across the yeast vacuolar membrane". en. In: *PLOS Genetics* 16.8 (Aug. 2020). Ed. by Widmar Tanner, e1008966. ISSN: 1553-7404. DOI: 10.1371/journal.pgen.1008966.

[10] Vadim Demichev et al. "DIA-NN: neural networks and interference correction enable deep proteome coverage in high throughput". en. In: *Nature Methods* 17.1 (Jan. 2020), pp. 41–44. ISSN: 1548-7091, 1548-7105. DOI: 10.1038/s41592-019-0638-x.

[11] Carlus Deneke, Reinhard Lipowsky, and Angelo Valleriani. "Complex Degradation Processes Lead to Non-Exponential Decay Patterns and Age-Dependent Decay Rates of Messenger RNA". en. In: *PLoS ONE* 8.2 (Feb. 2013). Ed. by Lev Tsimring, e55442. ISSN: 1932-6203. DOI: 10.1371/journal.pone.0055442.

[12] Daniela C. Dieterich et al. "Selective identification of newly synthesized proteins in mammalian cells using bioorthogonal noncanonical amino acid tagging (BONCAT)". en. In: *Proceedings of the National Academy of Sciences* 103.25 (June 2006), pp. 9482–9487. ISSN: 0027-8424, 1091-6490. DOI: 10.1073/pnas.0601637103.

[13] Mary K. Doherty et al. "Turnover of the Human Proteome: Determination of Protein Intracellular Stability by Dynamic SILAC". en. In: *Journal of Proteome Research* 8.1 (Jan. 2009), pp. 104–112. ISSN: 1535-3893, 1535-3907. DOI: 10.1021/pr800641v.

[14] Lars Dölken et al. "High-resolution gene expression profiling for simultaneous kinetic parameter analysis of RNA synthesis and decay". en. In: *RNA* 14.9 (Sept. 2008), pp. 1959–1972. ISSN: 1355-8382, 1469-9001. DOI: 10.1261/rna.1136108.

[15] E. Eriksson. "Natural reservoirs and their characteristics". English. In: *Geofisica International* 1.2 (Jan. 1961). Institution: Univ. of Stockholm, pp. 27–43.

[16] Erik Eriksson. "Compartment Models and Reservoir Theory". In: *Annu. Rev. Ecol. Syst.* 2.1 (Nov. 1971). Publisher: Annual Reviews, pp. 67–84. ISSN: 0066-4162. DOI: 10.1146/annurev.es.02.110171.000435.

[17] Eugenio F. Fornasiero et al. "Precisely measured protein lifetimes in the mouse brain reveal differences across tissues and subcellular fractions". en. In: *Nature Communications* 9.1 (Oct. 2018). Publisher: Nature Publishing Group, p. 4230. ISSN: 2041-1723. DOI: 10.1038/s41467-018-06519-0.

[18] Shenheng Guan et al. "Compartment modeling for mammalian protein turnover studies by stable isotope metabolic labeling". In: *Anal. Chem.* 84.9 (May 2012), pp. 4014–4021. ISSN: 0003-2700. DOI: 10.1021/ac203330z.

[19] Henrik M. Hammarén et al. "Protein-Peptide Turnover Profiling reveals the order of PTM addition and removal during protein maturation". en. In: *Nature Communications* 13.1 (Dec. 2022), p. 7431. ISSN: 2041-1723. DOI: 10.1038/s41467-022-35054-2.

[20] Dean E. Hammond et al. "Harmonizing Labeling and Analytical Strategies to Obtain Protein Turnover Rates in Intact Adult Animals". en. In: *Molecular & Cellular Proteomics* 21.7 (July 2022), p. 100252. ISSN: 15359476. DOI: 10.1016/j.mcpro.2022.100252.

[21] Robert Heise et al. "Flux profiling of photosynthetic carbon metabolism in intact plants". In: *Nat. Protoc.* 9.8 (Aug. 2014), pp. 1803–1824. ISSN: 1754-2189. DOI: 10.1038/nprot.2014.115.

[22] Marko Jovanovic et al. "Dynamic profiling of the protein life cycle in response to pathogens". en. In: *Science* 347.6226 (Mar. 2015), p. 1259038. ISSN: 0036-8075, 1095-9203. DOI: 10.1126/science.1259038.

[23] Liis Kolberg et al. "g:Profiler—interoperable web service for functional enrichment analysis and gene identifier mapping (2023 update)". In: *Nucleic Acids Research* 51.W1 (July 2023), W207–W212. ISSN: 0305-1048. DOI: 10.1093/nar/gkad347.

[24] Petri-Jaan Lahtvee et al. "Protein turnover forms one of the highest maintenance costs in Lactococcus lactis". In: *Microbiology* 160.7 (2014). Publisher: Microbiology Society, pp. 1501–1512. ISSN: 1465-2080. DOI: 10.1099/mic.0.078089-0.

[25] Wenxue Li et al. "Turnover atlas of proteome and phosphoproteome across mouse tissues and brain regions". en. In: *Cell* (Mar. 2025), S0092867425002090. ISSN: 00928674. DOI: 10.1016/j.cell.2025.02.021.

[26] Erik McShane et al. "Kinetic Analysis of Protein Stability Reveals Age-Dependent Degradation". In: *Cell* 167.3 (Oct. 2016), 803–815.e21. ISSN: 0092-8674. DOI: 10.1016/j.cell.2016.09.015.

[27] Michael E. Meadow et al. "Proteome Birthdating Reveals Age-Selectivity of Protein Ubiquitination". eng. In: *Molecular & cellular proteomics: MCP* 23.7 (July 2024), p. 100791. ISSN: 1535-9484. DOI: 10.1016/j.mcpro.2024.100791.

[28] Holger Metzler and Carlos A. Sierra. "Linear Autonomous Compartmental Models as Continuous-Time Markov Chains: Transit-Time and Age Distributions". en. In: *Mathematical Geosciences* 50.1 (Jan. 2018), pp. 1–34. ISSN: 1874-8953. DOI: 10.1007/s11004-017-9690-1.

[29] Aaron Meurer et al. "SymPy: symbolic computing in Python". en. In: *PeerJ Computer Science* 3 (Jan. 2017). Publisher: PeerJ Inc., e103. ISSN: 2376-5992. DOI: 10.7717/peerj-cs.103.

[30] Sebastian Niedenführ, Wolfgang Wiechert, and Katharina Nöh. "How to measure metabolic fluxes: a taxonomic guide for 13C fluxomics". In: *Curr. Opin. Biotechnol.* 34 (Aug. 2015), pp. 82–90. ISSN: 0958-1669. DOI: 10.1016/j.copbio.2014.12.003.

[31] Jang-Hyun Oh, Shun-Jia Chen, and Alexander Varshavsky. "A reference-based protein degradation assay without global translation inhibitors". eng. In: *The Journal of Biological Chemistry* 292.52 (Dec. 2017), pp. 21457–21465. ISSN: 1083-351X. DOI: 10.1074/jbc.M117.814236.

[32] Viridiana Olin-Sandoval et al. "Lysine harvesting is an antioxidant strategy and triggers underground polyamine metabolism". en. In: *Nature* 572.7768 (Aug. 2019). Number: 7768 Publisher: Nature Publishing Group, pp. 249–253. ISSN: 1476-4687. DOI: 10.1038/s41586-019-1442-6.

[33] Evgeny Onischenko et al. "Maturation Kinetics of a Multiprotein Complex Revealed by Metabolic Labeling". English. In: *Cell* 183.7 (Dec. 2020). Publisher: Elsevier, 1785–1800.e26. ISSN: 0092-8674, 1097-4172. DOI: 10.1016/j.cell.2020.11.001.

[34] Tegan A. Otto et al. "Nucleoporin Nsp1 surveils the phase state of FG-Nups". en. In: *Cell Reports* 43.10 (Oct. 2024), p. 114793. ISSN: 22111247. DOI: 10.1016/j.celrep.2024.114793.

[35] Alison Barbara Ross, Julian David Langer, and Marko Jovanovic. "Proteome Turnover in the Spotlight: Approaches, Applications, and Perspectives". en. In: *Molecular & Cellular Proteomics* 20 (2021), p. 100016. ISSN: 15359476. DOI: 10.1074/mcp.R120.002190.

[36] Cornelia Rücklé et al. "RNA stability controlled by m6A methylation contributes to X-to-autosome dosage compensation in mammals". en. In: *Nature Structural & Molecular Biology* 30.8 (Aug. 2023), pp. 1207–1215. ISSN: 1545-9993, 1545-9985. DOI: 10.1038/s41594-023-00997-7.

[37] Rudolf Schoenheimer and D. Rittenberg. "The Application of Isotopes to the Study of Intermediary Metabolism". en. In: *Science* 87.2254 (Mar. 1938), pp. 221–226. ISSN: 0036-8075, 1095-9203. DOI: 10.1126/science.87.2254.221.

[38] Rudolf Schoenheimer et al. "THE INTERACTION OF ANTIBODY PROTEIN WITH DIETARY NITROGEN IN ACTIVELY IMMUNIZED ANIMALS". en. In: *Journal of Biological Chemistry* 144.2 (July 1942), pp. 545–554. ISSN: 00219258. DOI: 10.1016/S0021-9258(18)72542-8.

[39] Ulrich Schubert et al. "Rapid degradation of a large fraction of newly synthesized proteins by proteasomes". en. In: *Nature* 404.6779 (Apr. 2000), pp. 770–774. ISSN: 0028-0836, 1476-4687. DOI: 10.1038/35008096.

[40] Björn Schwanhäusser et al. "Global quantification of mammalian gene expression control". en. In: *Nature* 473.7347 (May 2011), pp. 337–342. ISSN: 0028-0836, 1476-4687. DOI: 10.1038/nature10098.

[41] Min-Kyung Sung et al. "Ribosomal proteins produced in excess are degraded by the ubiquitin–proteasome system". en. In: *Molecular Biology of the Cell* 27.17 (Sept. 2016). Ed. by Thomas Sommer, pp. 2642–2652. ISSN: 1059-1524, 1939-4586. DOI: 10.1091/mbc.e16-05-0290.

[42] M. Terweij et al. "Recombination-induced tag exchange (RITE) cassette series to monitor protein dynamics in Saccharomyces cerevisiae". In: *G3 (Bethesda)* 3.8 (Aug. 2013), pp. 1261–72. ISSN: 2160-1836 (Electronic) 2160-1836 (Linking). DOI: 10.1534/g3.113.006213.

[43] Chongde Wu et al. "Global and Site-Specific Effect of Phosphorylation on Protein Turnover". en. In: *Developmental Cell* 56.1 (Jan. 2021), 111–124.e6. ISSN: 15345807. DOI: 10.1016/j.devcel.2020.10.025.

[44] Hsueh-Chi Sherry Yen et al. "Global Protein Stability Profiling in Mammalian Cells". en. In: *Science* 322.5903 (Nov. 2008), pp. 918–923. ISSN: 0036-8075, 1095-9203. DOI: 10.1126/science.1160489.

[45] Jamey D Young et al. "An elementary metabolite unit (EMU) based method of isotopically nonstationary flux analysis". In: *Biotechnol. Bioeng.* 99.3 (Feb. 2008), pp. 686–699. ISSN: 0006-3592. DOI: 10.1002/bit.21632.

[46] Roya Yousefi et al. "Influence of Subcellular Localization and Functional State on Protein Turnover". en. In: *Cells* 10.7 (July 2021), p. 1747. ISSN: 2073-4409. DOI: 10.3390/cells10071747.

[47] Jana Zecha et al. "Linking post-translational modifications and protein turnover by site-resolved protein turnover profiling". eng. In: *Nature Communications* 13.1 (Jan. 2022), p. 165. ISSN: 2041-1723. DOI: 10.1038/s41467-021-27639-0.

[48] Lijuan Zhang et al. "Method for Real-Time Monitoring of Protein Degradation at the Single Cell Level". en. In: *BioTechniques* 42.4 (Apr. 2007), pp. 446–450. ISSN: 0736-6205, 1940-9818. DOI: 10.2144/000112453.

[49] Janka Zsok et al. "Nuclear basket proteins regulate the distribution and mobility of nuclear pore complexes in budding yeast". en. In: *Molecular Biology of the Cell* 35.11 (Nov. 2024). Ed. by Anita Corbett, ar143. ISSN: 1059-1524, 1939-4586. DOI: 10.1091/mbc.E24-08-0371.